Longitudinal-acoustic-phonon softening in YS, LaS, and CeSe

M. M. Steiner*
Laboratorium für Festkörperphysik, Eidgenössische Technische Hochschule Hönggerberg CH-8093 Zürich, Switzerland and Department of Physics, University of California at San Diego, La Jolla, California 92093-0319

H. Eschrig
Zentralinstitut für Festkörperphysik und Werkstofforschung, Haeckelstrasse 20, Dresden, D-8027 Germany

R. Monnier
Laboratorium für Festkörperphysik, Eidenössische Technische Hochschule Hönggerberg, CH-8093 Zürich, Switzerland
(Received 9 October 1991)

The nonorthogonal tight-binding method of Varma and Weber is used to calculate the phonon spectra of YS, LaS, and CeSe, which exhibit strong anomalies in the longitudinal-acoustic branch, especially near the L point, where it crosses the transverse ones. The latter feature is found to arise from metal-metal interactions, which have their origin in the predominantly metal-derived electronic energy bands near the Γ point at the Fermi energy. With the addition of six Born-von Kármán force constants to model the short-range interactions, excellent agreement is obtained between theory and experiment in all three compounds.

I. INTRODUCTION

About a decade ago Weber studied the phonon anomalies in the refractory compounds (e.g., NbC, VN), which crystallize in the rocksalt structure, by using the nonorthogonal tight-binding (NTB) method presented a couple of years earlier by Varma *et al.*[1] He successfully calculated the longitudinal-acoustic (LA), phonon softenings in NbC,[2] and predicted changes in phonon anomalies on going from NbC to NbN (Ref. 2) or VN (Ref. 3), which were simultaneously confirmed by neutron scattering experiments. On going from NbC to VN (or NbN), the anomaly at the L point $(0.5, 0.5, 0.5)$ (expressed in reciprocal-lattice units), becomes much weaker, and the softening at wave vector $(0.65, 0.0, 0.0)$ becomes broader and moves to the X point $(1.0, 0.0, 0.0)$. These changes could be understood from differences in the underlying electronic structure of NbC and NbN or VN, which are mainly due to the addition of one more valence electrons in the nitrides. At about the same time neutron diffraction experiments revealed that YS, which also crystallizes in the rocksalt structure, exhibited similar phonon anomalies,[4] namely, softening of the LA, branches. Later LaS was found to show the same features as YS,[5] and more recently the same anomalies have been found in CeSe.[6] The main difference between the phonon spectra of NbC and those of these monochalcogenides is that at the L point, the softening has become so strong that the LA branch *crosses* the transverse acoustic (TA) branches. Further the LA anomaly at wave vector $(0.65, 0.0, 0.0)$ in NbC has become broader and moved to the X point. As the underlying electronic structure of these chalcogenides is similar to that of the refractory compounds we decided to study the anomalies using the NTB method.

II. METHOD OF CALCULATION

The electronic charge redistribution due to a distortion of the lattice can be viewed as a two-step process: the rigid motion of the valence shell with the ion core (neutral pseudoatom in an elemental solid), plus a deformation of the valence-electron cloud in order to adjust to the change in the local environment caused by the distortion. The effect of the first step on the total energy of the crystal can be modeled by a few *short*-range force constants, to give a smooth contribution to the dynamical matrix, $\underline{D}^{(\mathrm{bare})}$, which represents the unrelaxed motion of the ion cores. The second step involves the polarization of the valence-electron system, i.e., virtual transitions between occupied and empty valence band states induced by the change in potential due to the distortion. It is this term which is responsible for the anomalies and, as shown in detail in Refs. 1 and 7, in the NTB approach its contribution to the dynamical matrix, at wave vector $\mathbf{q}$ takes the form

$$D^{(2)}_{\kappa,\alpha;\kappa',\alpha'}(\mathbf{q}) = -\sum_{\substack{\mathbf{k},\mu,\mu' \\ \mathbf{k}'=\mathbf{k}+\mathbf{q}}} g^{\kappa\alpha}_{\mathbf{k},\mu;\mathbf{k}',\mu'} \frac{f_{\mathbf{k}',\mu'} - f_{\mathbf{k},\mu}}{e_{\mathbf{k},\mu} - e_{\mathbf{k}',\mu'}} g^{\kappa'\alpha'}_{\mathbf{k}',\mu';\mathbf{k},\mu} h(e_{\mathbf{k},\mu} - e_{\mathbf{k}',\mu'}) \quad , \tag{1}$$

where the superscript (2) indicates that we have only gone to second order in the relevant perturbation, i.e., the

valence part of the one-electron term in the Hamiltonian, which is *linear* in the displacements. κ, κ' are sublattice indices (e.g., Y or S), α, α' are Cartesian indices, μ, μ' valence band indices, $e_{\mathbf{k},\mu}$ is the energy of the μth valence band at $\mathbf{k}$, $f_{\mathbf{k},\mu}$ is the corresponding Fermi function, and $g^{\kappa\alpha}_{\mathbf{k},\mu;\mathbf{k}',\mu'}$ the electron-ion form factor or electron-phonon matrix element. We also include a cutoff factor or switch function, $h(e)$, which is 1 for $|e| < 1.2$ eV and vanishes otherwise, whose effect is discussed in the next section. Neglecting $h(e)$ for the moment, Eq. (1) has a simple interpretation. The first factor on the right-hand side of Eq. (1) is the matrix element associated with the destruction of the phonon of wave vector $\mathbf{q}$ and creation of an electron-hole pair, under momentum conservation. The second factor is just the $\{\mathbf{k}, \mu; \mathbf{k}', \mu'\}$ contribution to the bare electronic susceptibility or polarizability of the valence electrons, $\chi_0(\mathbf{q})$, which represents the propagation of this electron-hole pair. The electronic excitation then collapses and under momentum conservation recreating the phonon, as described by the third factor. By including this term in the full dynamical matrix we *dress* the bare phonons, represented by $\underline{D}^{(\mathrm{bare})}$, so as to allow for the effects due to the polarization of the valence-electron system by the phonon. In the NTB method the electron-phonon matrix elements have the form

$$g^{\tilde{\kappa}\alpha}_{\mathbf{k},\mu;\mathbf{k}',\mu'} = \sum_{\substack{\kappa,m \\ \kappa',m'}} A^{\dagger}_{\kappa,m;\mathbf{k},\mu}\left(\gamma^{\alpha}_{\kappa,m,\kappa',m';\mathbf{k}'}\delta_{\kappa,\tilde{\kappa}} - \gamma^{\alpha}_{\kappa,m,\kappa',m';\mathbf{k}}\delta_{\kappa',\tilde{\kappa}}\right) A_{\kappa',m';\mathbf{k}',\mu'} \quad , \tag{2}$$

where m, m' are orbital indices, and $A_{\kappa,m;\mathbf{k},\mu}$ the $\{m, \kappa\}$ coefficient of the μth eigenvector at $\mathbf{k}$. The three matrices γ^{α} are given by

$$\gamma^{\alpha}_{\kappa,m,\kappa',m';\mathbf{k}'} = \sum_{l-l'} \left(\nabla_{\alpha} H_{l\kappa m,l'\kappa' m'} - \epsilon \nabla_{\alpha} S_{l\kappa m,l'\kappa' m'}\right) e^{-i\mathbf{k}\cdot\mathbf{R}_{l\kappa,l'\kappa'}} \quad , \tag{3}$$

with $\epsilon = (e_{\mathbf{k},\mu} + e_{\mathbf{k}',\mu'})/2$. $H_{l\kappa m,l'\kappa' m'}$, $S_{l\kappa m,l'\kappa' m'}$ are the transfer and overlap integrals between the $\{m, \kappa\}$ orbital in the lth unit cell and the $\{m', \kappa'\}$ orbital in the l'th unit cell, and $\mathbf{R}_{l\kappa,l'\kappa'} = \mathbf{R}_{l\kappa} - \mathbf{R}_{l'\kappa'}$, where the vectors on the right-hand side define the equilibrium positions of the atoms. In Eqs. (2) and (3) the electron-phonon matrix elements have been written in terms of one-electron properties, i.e., the orbital coefficients of the equilibrium Bloch waves and the equilibrium, nonorthogonal tight-binding integrals and their derivatives. Neglecting crystal-field terms and using the Slater-Koster two-center representation for the integrals,[8] we can write

$$V_{l\kappa m,l'\kappa' m'} = \sum_{i=\{\sigma\pi\delta\}} V_i^{m,m'}(R_{l\kappa,l'\kappa'}) f_i^{m,m'}(q,p,r) \quad ,$$

where V represents either a transfer or overlap integral, and q, p, r the direction cosines from $l\kappa$ to $l'\kappa'$. This form means that V_i contains the full radial dependence of V, while f represents the angular part. This enables us to write the gradients in Eq. (3) as the sum of angular and radial derivatives. The former involve two-center integrals and trigonometric functions, and the latter can be expressed as sums of derivatives of two-center integrals. The derivatives of the two-center integrals are obtained by fitting the two-center integrals obtained from self-consistent calculations at compressed and expanded lattice constants to the form $V_i^{m,m'}(R) = V_{i,0}^{m,m'} \exp(\alpha R)$, so the logarithmic derivative with respect to R gives the inverse decay length, α. Except for the neglect of a possible $\mathbf{q}$ dependence of the gradients, this method of obtaining them fully accounts for screening and the variation in the exchange-correlation energy with the distortion, so the electron-phonon matrix elements in Eq. (1) are fully *screened*. As we have mentioned, $\underline{D}^{(2)}$ can be formally written as $g\chi_0 g$, where g is the screened electron-ion form factor. The overscreening with respect to the random phase approximation (RPA), which has the form $g\chi_0 g_0$, where g_0 is now the *bare* electron-ion form factor, is exactly compensated by a term involving the second derivative of the Hartree potential, which combined with the Coulomb interaction between the ion cores yields the dominant contribution to the short-ranged force constants mentioned at the beginning of this section.

Ideally, the energy bands of the system under consideration and the corresponding set of two-center integrals should be obtainable from one and the same self-consistent band-structure calculation. Using the optimized linear combination of atomic orbitals (LCAO) code developed by one of us,[9] we observed that matrix elements out to third nearest-neighbor-like and unlike atoms had to be included in order to obtain well-converged eigenvalues. The large number of parameters involved makes a direct implementation of the Varma-Weber formalism impractical. Therefore we obtained the two-center integrals from a fit of the bands to an NTB minimal basis set (d orbitals on the metal and s and p orbitals on the nonmetal), where only nearest-neighbor chalcogen-chalcogen, metal-metal and chalcogen-metal interactions were kept.[10] This means that in particular that the cerium $4f$ electron in CeSe is considered as be-

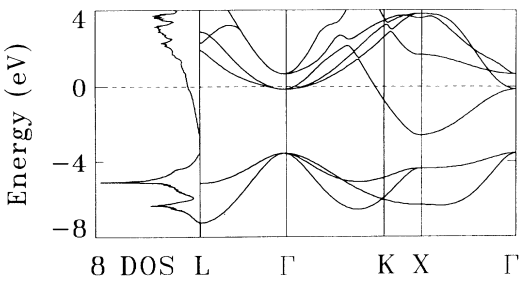

FIG. 1. YS energy bands along three high-symmetry directions and the density of states (leftmost panel). Energies in eV, density of states for both spins per unit cell per eV, the Fermi energy is at 0.0 eV. The S $3s$ band is at ~ -15 eV.

TABLE I. The NTB parameters and their logarithmic derivatives for (A) YS, (B) LaS, and (C) CeSe. The rows are (i) the transfer integrals, (ii) the overlap integrals, (iii) the logarithmic derivative of the transfer integrals, (iv) the logarithmic derivative of the overlap integrals. Transfer integrals are given in eV. We were not able to obtain reasonable values for some of the logarithmic derivatives, so they were set equal to zero. The weighted rms errors of the fits are (A) 0.14 eV, (B) 0.13 eV, and (C) 0.11 eV, and the maximum errors (at the L point) are (A) 0.39 eV, (B) 0.35 eV, and (C) 0.40 eV.

	$ss\sigma$	$sp\sigma$	$pp\sigma$	$pp\pi$	$d\,d\sigma$	$d\,d\pi$	$d\,d\delta$	$sd\,\sigma$	$p\,d\sigma$	$p\,d\pi$
					(A)					
(i)	−0.50	0.17	0.44	−0.15	−0.71	0.50	−0.07	−1.93	−1.16	2.03
(ii)	0.03	−0.01	0.01	0.01	0.11	−0.02	0.00	0.20	0.16	−0.15
(iii)	0.00	−1.33	−0.53	0.00	−0.71	−0.78	−0.86	−0.50	−0.40	−0.51
(iv)	0.00	−1.05	−0.09	0.00	−0.30	−0.36	0.00	−0.29	−0.25	−0.30
					(B)					
(i)	−0.47	0.16	0.34	−0.15	−0.64	0.54	−0.06	−1.74	−1.03	1.91
(ii)	0.03	−0.02	0.02	0.01	0.13	−0.05	0.03	0.21	0.10	−0.16
(iii)	0.00	−0.76	−0.79	−1.00	−0.62	−0.67	−0.82	−0.37	−0.53	−0.40
(iv)	0.00	−0.78	0.00	0.00	−0.37	−0.40	0.00	−0.19	−0.32	−0.30
					(C)					
(i)	−0.64	0.17	0.43	−0.16	−0.73	0.52	−0.07	−1.94	−1.14	2.06
(ii)	0.03	−0.01	0.01	0.01	0.11	−0.02	0.00	0.20	0.18	−0.11
(iii)	0.00	−1.00	−0.39	0.00	−0.47	−0.63	−0.70	−0.35	−0.39	−0.43
(iv)	0.00	0.00	−0.28	0.00	−0.40	−0.41	0.00	−0.23	−0.29	−0.42

ing part of the core, an assumption justified by the absence of f^0 peaks in the $3d$ core-level x-ray photoemission spectrum.[11] The LCAO band-structure calculations were nonrelativistic for YS (a = 5.49 Å) and semirelativistic (all relativistic effects included, except spin-orbit coupling) for LaS (a = 5.86 Å) and CeSe (a = 5.99 Å), and the von Barth–Hedin form for the local-density approximation to the exchange-correlation potential was used. In Fig. 1 we show the energy bands of YS in three symmetry directions, and the density of states in the leftmost panel. They agree reasonably well with older self-consistent calculations.[12] We give the resulting NTB parameters for the three compounds in Table I.

III. RESULTS

The calculation of $\underline{D}^{(2)}$ was performed using an adapted version of the tetrahedron method,[13] which enabled us to only consider virtual electron-hole excitations of less than a certain energy. By putting $g = 1$ in Eq. (1) we can calculate the bare susceptibility, $\chi_0(\mathbf{q})$. In NbC Gupta and Freeman,[14] and for YS Gupta,[15] found that the *intra*band part of $\chi_0(\mathbf{q})$ had peaks near the position of the anomalies, reflecting nesting of portions of the Fermi surface. However, calculations on Nb-Mo alloys[1] have shown that $\chi_0(\mathbf{q})$ usually only plays a secondary role in determining the $\mathbf{q}$ dependence of $\underline{D}^{(2)}$; much more significant is the $\mathbf{q}$ dependence of the electron-phonon matrix elements. For instance, it can be seen from Eqs. (1)–(3), that the intraband contribution to $\underline{D}^{(2)}(\mathbf{q})$ vanishes as $\mathbf{q} \to 0$, while the intraband part of $\chi_0(\mathbf{q}) \to N(E_f)$, the electronic density of states at the Fermi level. We found that only in the ΓL direction is $\chi_0(\mathbf{q})$ at all important in determining the $\mathbf{q}$ dependence of $\underline{D}^{(2)}$, a point we return to later. In Fig. 2 the dashed line is $\chi_0(\mathbf{q})$ for CeSe in the ΓX direction. For CeSe the total intraband bare susceptibility at $\mathbf{q}_L = (0.5, 0.5, 0.5)$ is $\sim 2.1\ \mathrm{eV}^{-1}$, i.e., more than twice the intraband part of $\chi_0(\mathbf{0})$, which is a much larger increase than usually found.

We now consider the effects of $h(e)$, see Eq. (1). The other two curves in Fig. 2 show $-\underline{D}^{(2)}_{\mathrm{Ce},x;\mathrm{Ce},x}(\mathbf{q})$, i.e., the $\underline{D}^{(2)}$ contribution to the LA branch. The top solid line includes all excitations within the three bands which cross the Fermi level, while for the bottom solid line we only considered the virtual excitations of less than 1.2 eV. The two curves are essentially related by a shift, and on including more *inter*band transitions, i.e., out of the nonmetal p complex into the metal d complex, the shift becomes larger but the form of $\underline{D}^{(2)}$ hardly changes. As the full dynamical matrix, $\underline{D}(\mathbf{q})$, is the sum of $\underline{D}^{(\mathrm{bare})}(\mathbf{q})$ and $\underline{D}^{(2)}(\mathbf{q})$, we can avoid the subtraction of large numbers in setting up $\underline{D}(\mathbf{q})$ by keeping the size of the $\mathbf{q} \to 0$ limit of $\underline{D}^{(2)}$ as small as possible. Therefore we have taken $h(e) = 0$ for $|e| > 1.2$ eV. [This choice for the cutoff is based on a balance between the number of allowed

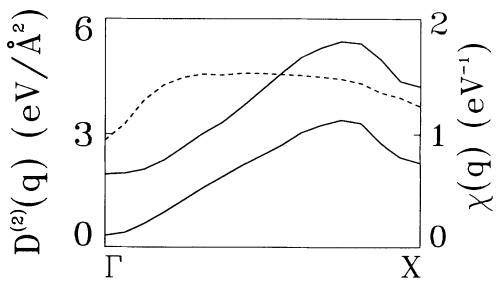

FIG. 2. The ΓX direction in CeSe, dashed line: $\chi_0(\mathbf{q})$ for CeSe; solid lines: $-\underline{D}^{(2)}_{\mathrm{Ce},x;\mathrm{Ce},x}(\mathbf{q})$ (see text for details).

virtual transitions and $\underline{D}^{(2)}(\mathbf{0})$.] The main effect of dropping the q-independent part of $\underline{D}^{(2)}(\mathbf{q})$ is to renormalize the short-range force constants used in $\underline{D}^{(\mathrm{bare})}(\mathbf{q})$.

We modeled the short-range part of the dynamical matrix, $\underline{D}^{(\mathrm{bare})}(\mathbf{q})$, by six force constants, two between nearest-neighbor metal, two between nearest-neighbor metal and nonmetal, and two between next nearest-neighbor metal nonmetal ions. We did not include force-constants between the lighter nearest-neighbor nonmetal ions, as the optical phonons do not exhibit anomalous behavior, and so we only reproduced their center of mass. In Fig. 3 we compare our results (solid lines) with experimental data (symbols). To illustrate the effect of $\underline{D}^{(2)}(\mathbf{q})$ we also show the acoustic spectra when $\underline{D}^{(\mathrm{bare})}(\mathbf{q})$ alone is diagonalized (dotted line). It is clear that the changes of the TA branches due to $\underline{D}^{(2)}$ are weaker and smoother than the corresponding changes in the LA branch. In Figs. 4(a)–4(c) we show the acoustic spectra for the three chalcogenides.

While the differences between the phonon spectra of NbC and NbN could be explained by changes in the electronic structure due to the addition of one more electron per unit cell, the chalcogenides and NbC are valence isoelectronic, so we must look elsewhere for the cause of the differences in the anomalies, mentioned in the Introduction. One difference is the increase of the lattice constant on going from NbC to YS (4.47 to 5.49 Å), but this is nearly fully compensated for by an increase in the radial extent of the S $3p$ wave function compared to the C $2p$ wave function, as is reflected by the closeness of the NTB parameters for the two materials. Another major difference is that Y is to the left of Nb in the Periodic Table and S is to the right of C, which means that the difference between the onsite Y $4d$ level and the S $3p$ level is greater than the Nb $4d$–C $2p$ difference. As we can see in Fig. 1 this leads to the metal d and nonmetal p bands being well separated in YS, whereas in NbC they overlap. This results in two changes: (a) the energy-momentum dispersion of the electron bands near the Γ-point changes, which leads to nearly a doubling of the bare intraband susceptibility at $\mathbf{q}_L$ from $\sim 1.2\ \mathrm{eV}^{-1}$ in NbC to $\sim 2.2\ \mathrm{eV}^{-1}$ in YS and (b) a reduction in the amount of p character in the bands near the Γ point at the Fermi level on going from NbC to YS, which leads to slightly different electron-phonon matrix elements [see Eq. (2)]. The end result is an increase in the magnitude of $\underline{D}^{(2)}(\mathbf{q})$, especially the *off*-diagonal elements, with respect to NbC. At the L point $(0.5, 0.5, 0.5)$, in the rock-salt structure, the metal and nonmetal motions are decoupled, i.e., only the heavier metal ions are displaced by an acoustic L-point phonon. This means we only have to consider the metal-metal block of the full dynamical matrix, which at the L point, because of the equivalence of the three Cartesian directions, has the form

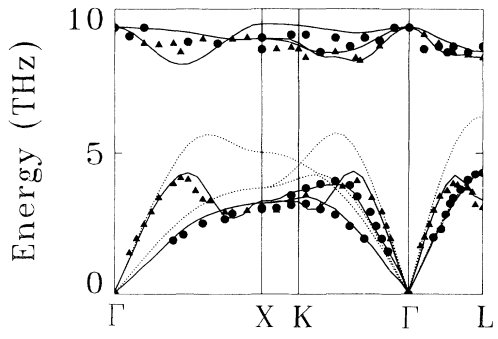

FIG. 3. A comparison of our results for the phonon dispersion curves (solid lines) for YS with experimental results (triangles: longitudinal, circles: transverse). The dotted lines are the results of diagonalizing $\underline{D}^{(\mathrm{bare})}$ rather than the full dynamical matrix.

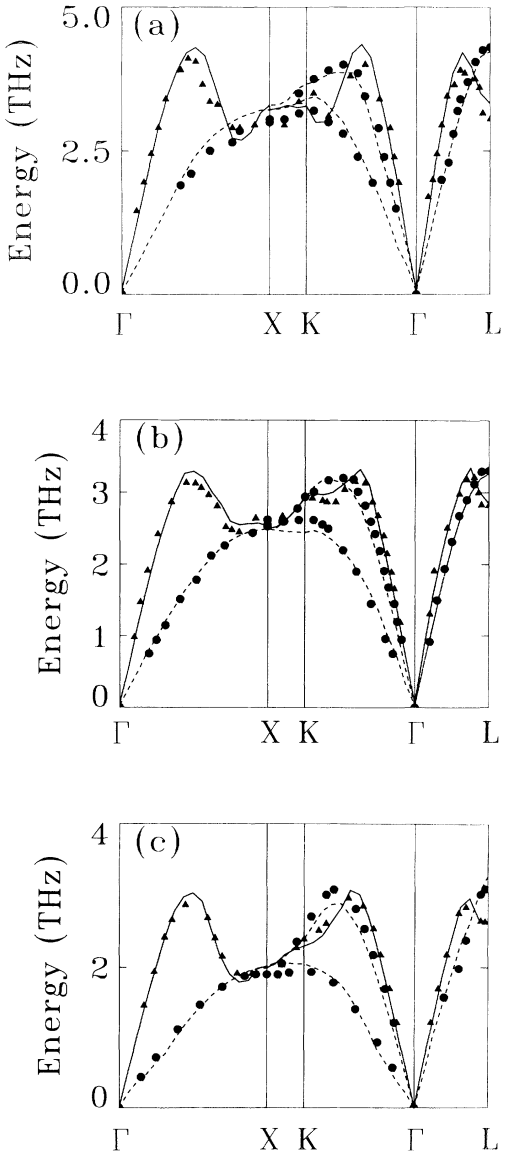

FIG. 4. The acoustic phonon spectra for (a) YS, (b) LaS, and (c) CeSe. The lines are our results (solid: longitudinal, dashed: transverse), and the symbols are neutron scattering results (triangles: longitudinal, circles: transverse).

$$\begin{pmatrix} a & b & b \\ b & a & b \\ b & b & a \end{pmatrix}, \tag{4}$$

where a and b result from summing $\underline{D}^{(\mathrm{bare})}(\mathbf{q})$ and $\underline{D}^{(2)}(\mathbf{q})$. The resulting three acoustic frequencies are proportional to $\sqrt{a+2b}$ (LA) and a doubly degenerate $\sqrt{a-b}$ (TA). Normally b is positive, so the LA frequency is larger than the TA frequencies. However, for the chalcogenides $\underline{D}^{(2)}(\mathbf{q})$, as we have explained above, becomes sufficiently negative as $\mathbf{q} \to \mathbf{q}_L$, for b to change sign, leading to the observed crossing of the TA branches by the LA branch.

On the other hand the other two anomalies have essentially the same origin as in NbC. The anomalies near the X point in YS, and $(0.65, 0.0, 0.0)$ in NbC, are both driven by the increase in p character of the electron bands near the X point, which leads to enhanced couplings due to $\nabla p\, d\sigma$ interactions at the wave vectors of the anomalies, see Ref. 7. In contrast to the Γ point, near the X point the character of the electronic bands and their dispersion is similar in both NbC and the chalcogenides. Finally, even though in YS we overestimate the strength of the LA anomaly in the ΓKX direction, near $\mathbf{q} = (0.6, 0.6, 0.0)$ we do find the same trend as experiment; i.e., the anomaly becomes weaker on going from YS to LaS to CeSe.

IV. SUMMARY

In summary, we have found that the NTB method of Varma and Weber gives a good description of the softening of the LA branches in YS, LaS, and CeSe. By considering only low-energy electronic excitations we concentrate on calculating the anomalous part of the dynamical matrix, which arises from the valence electrons' response to the phonon distortion, while the normal smooth part is modeled by six short-range springs. While the ΓX and ΓKX anomalies are basically the same as in the refractory compounds, the L-point anomaly in the chalcogenides is found to be stronger because of changes in the electronic structure near the zone center, which enhances $\underline{D}^{(2)}(\mathbf{q})$, for $\mathbf{q} \approx \mathbf{q}_L$. In this case both the bare susceptibility and the electron-phonon matrix elements are important in determining the strength of the valence-electron response to the phonon, and thus the degree of softening.

ACKNOWLEDGMENTS

We are grateful to the authors of Ref. 6 for letting us use their unpublished data on CeSe. We have greatly benefited from discussions with A. Dönni and W. Weber.

*Mailing address: Theoretical Division MS-B262, Los Alamos National Laboratory, Los Alamos, NM 87545.

[1] C. M. Varma, E. I. Blount, P. Vashishta, and W. Weber, Phys. Rev. B **19**, 6130 (1979); C. M. Varma and W. Weber, *ibid.* **19**, 6142 (1979).

[2] W. Weber, in *Superconductivity of d- and f-Band Metals*, edited by H. Suhl and M. B. Maple (Academic, New York, 1980).

[3] W. Weber, P. Rödhammer, L. Pintschovius, W. Reichardt, and A. N. Christensen, Phys. Rev. Lett. **43**, 868, (1979).

[4] P. Rödhammer, W. Reichardt, and F. Holtzberg, Phys. Rev. Lett. **40**, 465, (1978).

[5] W. Reichardt (unpublished).

[6] A. Dönni, A. Furrer, W. Bührer, and F. Hulliger (unpublished).

[7] W. Weber, Habilitation Thesis of the Fakultät für Physik, Universität Karlsruhe; in *Electronic Structure of Complex Systems*, edited by P. Phariseau and W. Temmerman (NATO-ASI Series, Plenum, New York and London, 1984).

[8] J. C. Slater and G. F. Koster, Phys. Rev. **94**, 1498 (1954).

[9] H. Eschrig, *Optimized LCAO Method and the Electronic Structure of Extended Systems* (Akadamie-Verlag, Berlin 1988).

[10] The inclusion of the S $3d$ (Se $4d$) states was found to be essential to the convergence of the the LCAO calculations, also the nonmetal d partial density of states in the region near the Fermi level is larger than in NbC (Refs. 12 and 15). This suggested that our reduction of the basis set to s, p on the nonmetal, might not be valid, but additional calculations of the electron-phonon matrix elements, with the S $3d$ orbitals included, showed practically no difference.

[11] R. Lässer, J. C. Fuggle, M. Beyss, M. Campagna, F. Steglich, and F. Hulliger, Physica **102B**, 360 (1980).

[12] J. A. Appelbaum and D. R. Hamann, Inst. Phys. Conf. Ser. **39**, 111 (1978); K. Schwarz and E. Wimmer, J. Phys. F **10**, 1001 (1980).

[13] J. Rath and A. J. Freeman, Phys. Rev. B **11**, 2109 (1975).

[14] M. Gupta and A. J. Freeman, Phys. Rev. B **14**, 5205 (1976).

[15] M. Gupta, Phys. Rev. B **20**, 4334 (1979).